JOURNAL OF PROPULSION AND POWER
Vol. 17, No. 4, July–August 2001

Combustion Behavior and Flame Structure of XM46 Liquid Propellant

Y.-P. Chang,* E. Boyer,* and K. K. Kuo†
Pennsylvania State University, University Park, Pennsylvania 16802

This investigation was focused on the combustion behavior of XM46. The regression rate of XM46 has been characterized up to 207 MPa, displaying a complex burning behavior with both negative pressure exponent and plateaulike behavior. The flame structure displayed three different stages: 1) nearly simultaneous decomposition of both hydroxylammonium nitrate (HAN) and triethanol ammonium nitrate initiating in the liquid to produce gases around 300°C, 2) breakdown of heavy opaque intermediate molecules into transparent species, and 3) reaction of transparent species to form final products in the luminous flame. The feeding tests showed peculiar flashback phenomena, believed to be related to the interaction between gas-phase radicals and unburned liquid propellant. Pyrolysis tests of XM46 were conducted in a specially designed pyrolyzer used in conjunction with a gas chromatograph/mass spectrometer. The major pyrolysis products observed were NO, N_2O, N_2, CO_2, CO, H_2O, HCN, and C_2H_4 when pyrolyzed at temperatures between 130 and 540°C. The pressure dependency of the burning rate of the HAN-based liquid propellant is highly nonlinear. Water evaporation has a noticeable effect on combustion characteristics of XM46. Gas dissolution/desorption could also affect the burning rate. The type of fuel ingredient was found to have a significant effect on the overall burning characteristics.

Introduction

LIQUID propellant (LP) gun systems, using hydroxylammonium nitrate (HAN) as one of the major propellant ingredients, were first proposed more than 10 years ago.[1,2] The attractive features include high energy, high density, low glass-transition point, relative stability, low toxicity, and easy demilitarization and disposal. HAN-based propellants are also being considered as a replacement for hydrazine in space propulsion systems.[3–6] Because of their potential in many propulsion applications, HAN-based propellants have been of major interest to many researchers.

The XM46 LP, consisting of hydroxylammonium nitrate (HAN, NH_3OHNO_3, 60.8%), triethanol ammonium nitrate [TEAN, $(HOCH_2CH_2)_3NHNO_3$, 19.2%], and water (20% by weight), was developed as a potential LP for gun propulsion systems. The chemical structures of HAN and TEAN are shown in Fig. 1.

Many researchers have used different ways to measure the burning rate of XM46. Oberle and Wren[7] deduced the burning rate from the pressure curves measured in closed-bomb tests. They found a pressure exponent of nearly 2. The unusually high pressure-exponent was attributed to underestimation of burning surface area, which was assumed to be the cross-sectional surface area of the sample holder. McBratney and Vanderhoff[8] added gelling agents into LP to reduce the possible surface agitation. The pressure exponent they found was considerably lower than that of Oberle and Wren,[7] and a slope break was observed around 70 MPa. Vosen[9] used a strand burner to measure the burning rate of both an ungelled HAN–water solution and LGP 1846 (which has the same composition as XM46). He found a decreasing trend of burning rate with increasing pressure from 7 to 30 MPa and staged combustion characteristics. He proposed the following physical model of the LGP 1846 combustion: 1) The first stage of combustion is HAN decomposition, in which TEAN does not participate in the reaction. 2) Later in the combustion event, molten TEAN reacts with HAN decomposition products producing a luminous flame. Vosen[10,11] also hypothesized that the decrease in burning velocity with increasing pressure is controlled by surface instabilities of liquid–gas interface, which is a function of the density ratio across the interface. Koch et al.[12] designed and built an LP strand burner with a precise liquid feeding system. Instead of containing a liquid strand inside a tube or straw and allowing the flame to propagate down into the tube, the liquid was fed upward to stabilize the burning surface at the exit port of the feeding tube. In this manner, the heat loss to the tube wall and confinement effects could be minimized. The system yielded good burning rate results for nitromethane.[13] Jennings et al.[14] attempted to use this technique to measure the burning rate of XM46, but found that the burning surface could not be stabilized on the port of the feeding tube, no matter how fast the liquid was fed. The reaction front kept regressing down into the tube at all feeding rates attempted, and a dark-colored cone formed above the regression surface.

Reaction kinetics of XM46, HAN, or similar LP blends have been the focus of various researchers. Klein[15] conducted a mechanistic study of the ignition and combustion of liquid gun propellant (LGP) 1845 [63.2% HAN, 20.0% TEAN, and 16.8% water] using an accelerating rate calorimeter. He found that the reaction consists of three stages: 1) formation of nitronium ions (NO_2^+) in the liquid phase initiating the HAN decomposition, 2) start of ignition as HAN decomposition products react with TEAN, and 3) subsequent combustion of the gaseous products. Lee and Thynell[16] and Thynell and Kim[17] studied the thermal decomposition of solid HAN and HAN–water solutions and found that HAN decomposition consists of several stages: 1) Proton transfer and subsequent reactions occur while water evaporates as the sample heats up. As the critical concentration of HAN is reached, the reaction rate is greatly accelerated, forming a pool of highly reactive HONO and HNO species. 2) There is evolution of gas species and depletion of HAN. 3) Last are the reactions among HAN decomposition products. The oscillatory nature of species evolution profiles was observed, which was attributed to the autocatalytic behavior of nitrous acid. At higher pressures, they found a second peak in the gas evolution profile. A detailed HAN decomposition mechanism was summarized, but no rate constants were provided. Cronin and Brill[18] investigated the thermolysis of LGP 1845 by measuring the temperature of the heated sample and evolved gaseous species at different heating rates and pressures. For LGP 1845, they found four main events during the process. First, water evaporates and increases the concentration of the sample. Second, proton transfer between the cation and anion of

Presented as Paper 00-0706 at the AIAA 38th Aerospace Sciences Meeting and Exhibit, Reno, NV, 10–13 January 2000; received 7 April 2000; revision received 13 January 2001; accepted for publication 19 February 2001.

*Ph.D. Candidate, Department of Mechanical and Nuclear Engineering. Student Member AIAA.

†Distinguished Professor, Mechanical Engineering, and Director, High Pressure Combustion Laboratory. AIAA Fellow.

HAN initiates the decomposition of HAN. This happens at around 160–170°C. The third step is the partial decomposition of TEAN at around 240–250°C. The last step is the ignition of the sample. Lee and Litzinger[19] examined the combustion process of XM46 at extremely high heating rates using a high heat-flux CO_2 laser. Their results showed that in the early stage of reaction, it was primarily HAN that reacted and TEAN in the later stage. The evolved gas species suggested the early decomposition of TEAN. Relatively little work has been done on the reaction kinetics of TEAN. Beyer[20] used a shock tube to measure the activation energy of TEAN powder under oxygen/Ar and nitrous oxide/Ar environments. The activation energy of solid TEAN provided by Beyer is very close to what was reported for aqueous HAN.[21] He suggested that the measured activation energy (9.6 kcal/mol in nitrous oxide/Ar) was largely due to the melting of TEAN; that is, the melting might be the rate limiting step, inasmuch as the heat of fusion for TEAN is 149 J/g or 7.55 kcal/mol.

This work is the continuation of previous studies.[14,22] The burning-rate curve has been extended to a pressure of 207 MPa (30,000 psi) using a specially designed ultra-high-pressure strand burner. The temperature profiles of the combustion zone were measured at different pressures. Comparing the results of this study and our previous data revealed insights to the burning-rate data, physicochemical processes, and peculiar phenomena of XM46.

Experimental Approach

LP Strand Burner (LPSB)

A specially designed LP strand burner (LPSB), which contains an accurate liquid feeding system, was utilized to study intrinsic burning behavior of LPs. The detailed description of the setup can be found elsewhere.[23] The schematic diagram is shown in Fig. 2.

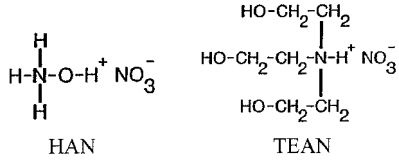

Fig. 1 Chemical structure of HAN and TEAN.

In feeding tests, the LPs were fed up into a tube to establish a stable flame at the port of the tube. Once the stable flame was established, one could deduce the burning rate from the preset feeding speed.

The traditional static tests of stagnant LP strands can also be performed in the LPSB. In static tests, experiments were conducted by filling LP into a quartz tube (7 mm inside diameter) or a thin-walled cylindrical straw made from a combustible wax paper. Each method has its own advantages and disadvantages. By using the quartz tube, the propellant flame is confined in a one-dimensional reaction zone. The combustion product gases are forced to accelerate in the vertical direction, resulting in a stretched reaction zone. This stretching effect is beneficial for observation of the combustion phenomena and is helpful to provide a comparison with one-dimensional model simulations. In contrast, the unconfined burning of LP in combustible straws minimizes heat loss from the propellant flame to the tube wall, thereby allowing the LPs to burn at their intrinsic burning rates.

The optically accessible windows of the LPSB allow the visual observation of the whole combustion event and the use of nonintrusive diagnostic techniques. Also, in some tests, thermocouples were installed in the center of the quartz tube to measure the temperature profile across the burning surface of the propellant as well as the gaseous flame. Although the test chamber itself can sustain pressures up to 70 MPa, all tests conducted in this chamber were at pressures less than 35 MPa due to the limitations of the optically accessible windows. The tests at pressures higher than 35 MPa were performed in the ultra-high-pressure strand burner.

Ultra-High Pressure Strand Burner (UHPSB)

Conventional vented strand burners generally have pressure limits of less than 70 MPa (~10,000 psi). However, pressures generated inside gun chambers are much higher, possibly exceeding 700 MPa (~100,000 psi). To examine the combustion behavior at high pressures, an ultra-high-pressure strand burner (UHPSB) was designed, constructed, and tested. Detailed description of this setup can be found elsewhere.[23] The schematic diagram of the UHPSB is shown in Fig. 3.

The UHPSB allows strand burning rates of propellants to be measured at pressures up to 207 MPa (30,000 psi). Solid or liquid

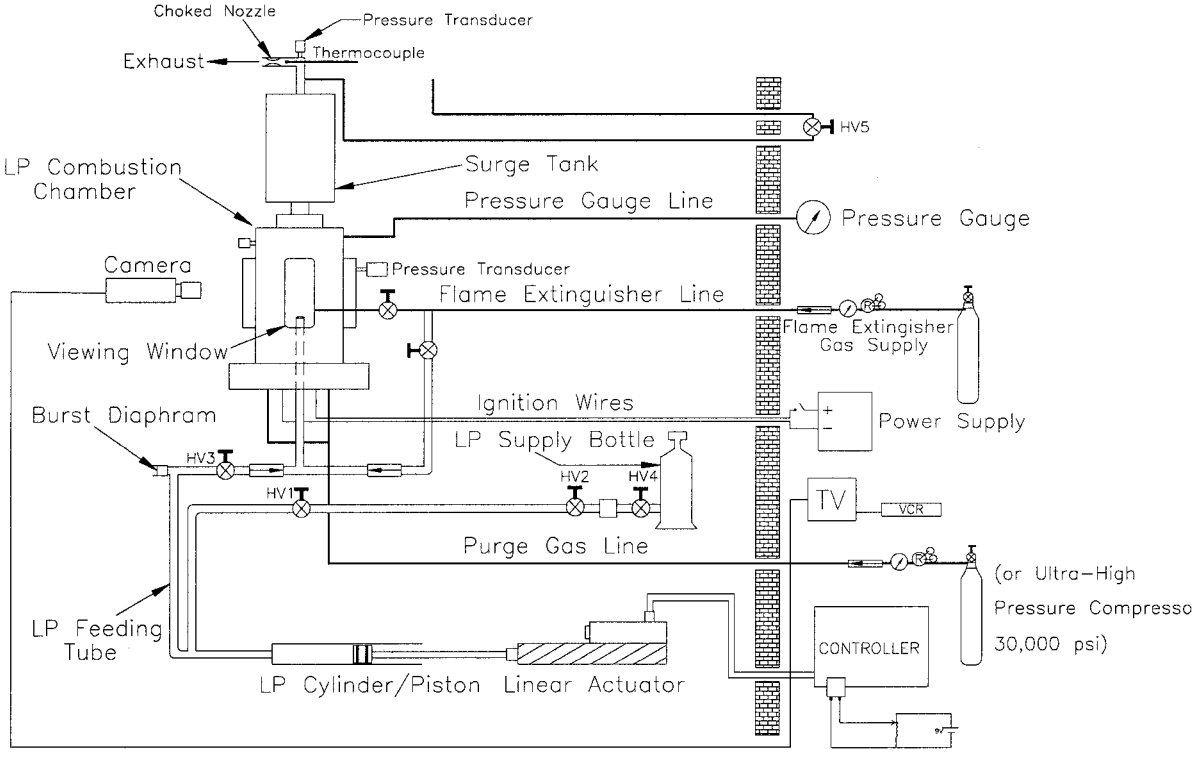

Fig. 2 Schematic diagram of LPSB.

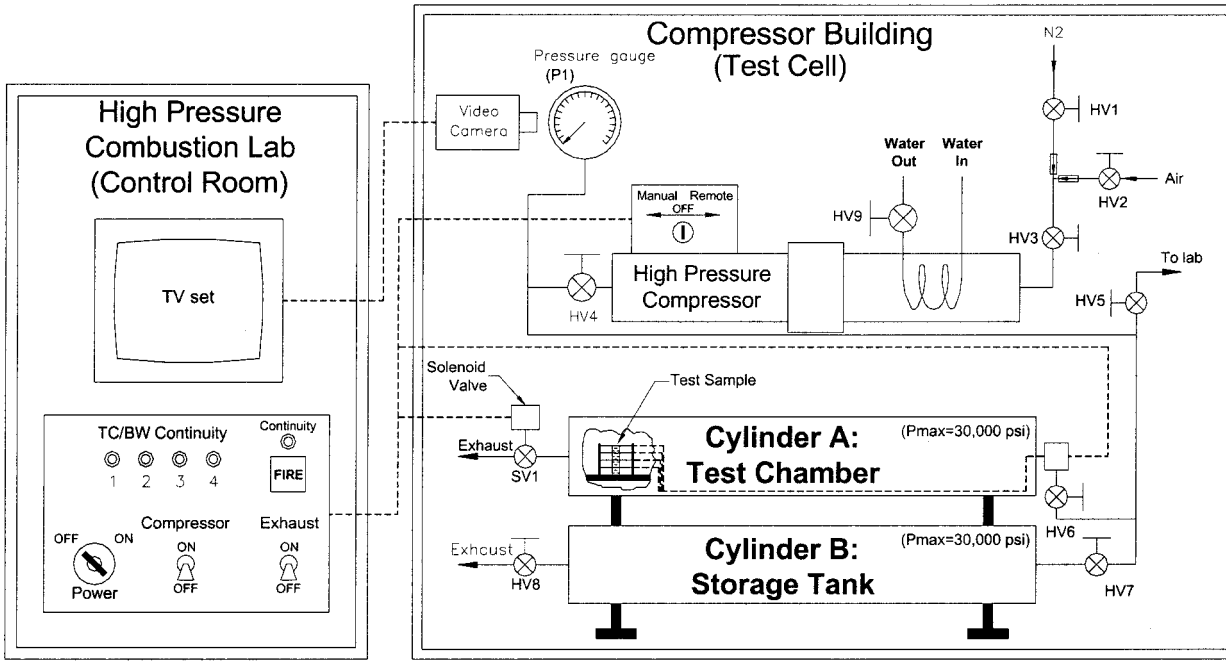

Fig. 3 Schematic diagram of UHPSB.

samples up to 65 mm long can be tested. LP or gelled propellant strands can be contained in either quartz tubes or combustible straws. To pass ignition power and diagnostic signals through the high-pressure chamber wall, a custom-made eight-wire electrical feedthrough was utilized. A total of three thermocouples (TCs), or up to four break wires (BWs) per sample, can be monitored using this setup. The control panel allows operation and observation of a number of important functions from a remote site, including 1) compressor power control for chamber pressurization, 2) exhaust valve actuation, 3) electrical continuity test on TC/BW/ignition, 4) trigger output from ignition switch for data acquisition system activation, and 5) variac or dc power source control for igniter power input.

Segments of Bussman 0.25-A fuse wire threaded through the propellant strands were utilized as BWs. Burning rate was deduced by measuring the time delay between burnthrough of adjacent wires. Four holes were drilled or punched at known intervals in combustible straws or quartz tubes, and the BWs were passed through these holes. The holes were then sealed with a dot of epoxy to contain the LPs. TC mounting was similar to the BW mounting. As configured, the UHPSB used a nichrome hot-wire ignition system. Electrical energy was supplied by either a variac or dc power source at the control panel.

Because the test chamber was adapted from a high-pressure compressor storage tank with a length of approximately 6 ft (1.83 m) and a 4 in. (101.6 mm) inside diameter, the internal volume is very large. Therefore, pressure change due to heat and product gases released during the combustion event was negligible. The high-pressure gas environment for combustion was determined by the gas input source to the compressor. The gas environment used for XM46 tests was generally nitrogen, but other gases such as air or argon could easily be substituted.

The control and data acquisition systems are located in another building apart from the one containing the UHPSB test chamber. Both the compressor and the exhaust solenoid valve (SV1) can be remotely operated to increase or decrease the chamber pressure to the desired level. To run an experiment, the igniter power input is set, then the test triggered.

Gas Chromatograph/Mass Spectrometer with Flash Pyrolyzer

A Shimadzu QP-5000 gas chromatograph/mass spectrometer (GC/MS) system coupled with a Shimadzu PYR-4A high-temperature pyrolyzer was used to identify and quantify the pyrolysis species of propellants at temperature of interest. A small amount of sample was placed in a platinum cup and dropped into the pyrolyzer at a preset temperature. The maximum temperature of the pyrolyzer is 800°C. The gas evolved was carried into the GC subsystem by helium, where the different compounds in the gas were separated by the capillary column. The separated compounds passed through the transfer interface and went into the MS subsystem. The subsystem ionized and/or fragmented the compounds by electron beam and scanned through the specified mass-to-charge ratio M/Z range to determine the mass spectrum of the compound. The MS subsystem can scan the ions with M/Z between 10 and 700 at a maximum scanning rate of 6000 atomic mass units/s. The mass spectrum measured was compared with spectra of known substances by software to identify the species. Each compound was quantified by integrating the area under its chromatograph peak and comparing the area with the calibration constant obtained using the pure substance.

Results

Burning-Rate Measurement in Static Tests

The burning rate vs pressure curve for XM46 was extended up to 207 MPa with the test results obtained from the UHPSB using combustible straws. The extended results together with previous reported burning-rate data by other investigators are shown in Fig. 4. As mentioned in the "Experimental Approach" section, the burning rate for tests conducted in the UHPSB was deduced by measuring the time delay between burnthrough of adjacent BWs. Therefore, the reported burning rates are apparent burning rates. Furthermore, in both UHPSB and LPSB, the effect of liquid agitation near the reaction front may contribute to the increase of the actual burning surface area, which changes with respect to time. The apparent burning rate reported in this study corresponds to the deduced linear regression rate parallel to the tube/straw axis. In spite of the fact that the apparent burning rate may differ from the actual burning rate to some extent, it is still extremely useful data for LP propulsion applications because the tube cross-sectional area and liquid density are both known. The total mass burning rate of the LP at a given pressure can be determined by the product of the apparent burning rate to these two known parameters.

In Fig. 4, the curve fit for the present data displays four different burning-rate regimes. At low pressures, the rate of regression increased with rising pressure, reaching a maximum close to 23 cm/s at 7 MPa. Beyond 7 MPa, the regression rate then decreased with

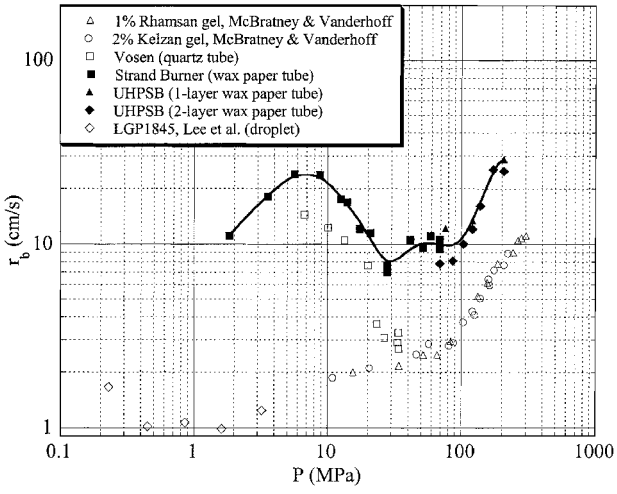

Fig. 4 XM46 burning rate as function of pressure, $T = T_{room}$.

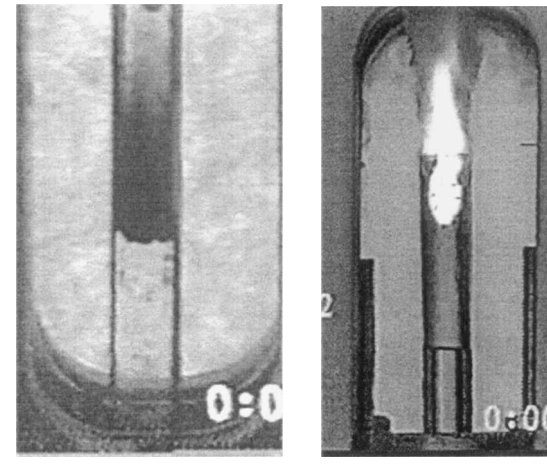

17.3 MPa **31.1 MPa**

Fig. 5 Quartz tube tests of XM46.

increasing pressure. A minimum regression rate was seen close to 28 MPa. At pressures between 28 and 100 MPa, burning rate is nearly constant. Finally, at pressures beyond 100 MPa, burning rate increased with pressure again. Note that the burning rate of neat XM46 obtained in this investigation is significantly higher than those reported by McBratney and Vanderhoff[8] at the U.S. Army Research Laboratory for slightly gelled propellants. This indicates the strong influence of gelling agents on the combustion behavior of LP. In addition, for the low-pressure regimes, the present data are higher than those of Vosen.[11] The difference is believed to be caused by the greater heat loss from the reaction zone to his rectangular quartz channel. The single-droplet-burning rate of LGP 1845 (HAN 63.2 wt%, TEAN 20.0 wt%, water 16.8 wt%) measured by Lee et al.[24] is also shown in Fig. 4 for comparison purpose. In the Lee et al. study, a single droplet was supported by a quartz fiber, which could have a significant energy sink effect when the droplet is in the burning mode. Before the droplet started to burn, Lee et al. observed pronounced droplet swelling phenomena due to internal bubble formation caused by bulk reaction within the droplet. We believe that these processes are caused by energy transfer from the quartz fiber to the LP. The thermal diffusivity value of a regular quartz fiber is many times higher than that of LGP 1845. As stated by Lee et al., "The effective droplet burning rate involved both reaction within the bulk liquid causing bubble formation and bursting, dominating the process at low pressures. . . ." In addition, their droplet was always exposed to a hot-gas environment; therefore, the ignition heat source was always present. Thus, the Lee et al. burning-rate data can exist for pressures as low as 0.2 MPa, whereas in the present study, no self-sustainable combustion was observed below the pressure of 1.82 MPa (265 psia).

Combustion Phenomena Observation

To observe the combustion phenomena and flame structure, static and feeding tests were also performed in cylindrical quartz tubes. Because of the confinement of the tube wall, all of the product gases could only flow in the upward direction. This one-dimensional situation allowed a better observation of the combustion event and enhanced understanding of the reaction mechanism. All visual observations were conducted in the LPSB.

Typical pictures of static burning events at two different pressures are shown in Fig. 5. In low-pressure regimes (below 28 MPa), no luminous flame was present. The decomposition of the LP produced dark smoke with some liquid droplets entrained within the gases; these droplets coated the interior surfaces of the tube and combustion chamber. This smoke formed a dark opaque zone right above the decomposition front. For tests at higher pressures, the dark smoke turned into transparent gases at some axial distance above the decomposition front. The length of the dark opaque zone decreased with increasing pressure, eventually shrinking to the thickness of the

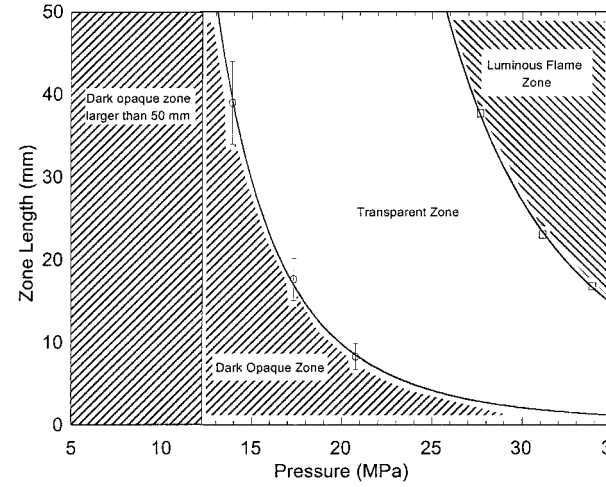

Fig. 6 Pressure dependency of height of reaction zones of XM46.

liquid meniscus, becoming almost negligible. The luminous flame did not appear above the transparent zone until the pressure was greater than 28 MPa. Similarly, the length of the transparent zone (between the end of dark opaque zone and luminous flame front) decreased as the pressure was increased. The length of different zones at different pressures is shown in Fig. 6.

Some peculiar phenomena were observed in feeding tests. First, the reaction front could not be stabilized at the exit port of the feeding tube, no matter how fast the liquid was fed. Furthermore, the reaction front propagated down into the feedline at nearly constant speed for all of the feeding rates tested. In the 27.7-MPa case, for example, the burnback always occurred at a slightly higher ($\sim$1.6 cm/s) regression rate than the feeding rate. The data from tests at other initial chamber pressures showed very little difference in their burnback velocities into the moving LP from those of the 27.7-MPa test condition. Though the tube tests (unfed) showed an increase in burning rate as the pressure lowered below 28 MPa, the rate at which the burnback phenomenon occurred in feeding tests remained largely constant, even at lower pressures.

Second, a black cone was formed atop the reaction front, as shown in Fig. 7. The black cone was not present at all in the static tube tests. The height of this cone increased as the feeding rate increased. This is clearly seen in Fig. 7a (a 7.6-cm/s feeding rate test) and Fig. 7b (a 15.2-cm/s feeding rate test). In Fig. 7a, the luminous flame initiates from the tip of the black cone. Figure 7b, however, shows that a luminous flame was not always directly in contact with the apex of this cone. In most tests at higher pressures, these two inverted cones traveled together.

Temperature Measurements of Reaction Zone

The temperature distribution of reaction zone was measured using S-type TCs with a quartz tube as an LP holder. The measurements were performed in both feeding and static test conditions. The burning rate, however, was very fast such that the thermal wave thickness was on the order of a few micrometers. Therefore, the subsurface temperature profile and the surface temperature could not be resolved by 25-μm TCs. Figure 8 shows typical temperature–time traces in the reaction zone for static tests at two different pressures. For each test, two TCs were installed at two axial locations. At a relatively low pressure of 13.8 MPa (2000 psig), there was no luminous flame. As shown in Fig. 8a, the temperature of the dark smoke (the initial temperature plateau) was around 300°C. Later in the event, both TCs, although at different locations, reached the same maximum temperature (about 600°C) at the same time. On the video, this corresponded to the sudden clearing of the dark smoke after the regression front passed through the whole column of liquid and reached the bottom of the tube. Because the whole column of liquid was consumed by the advancement of the decomposition front, the gas in the tube at this stage became nearly stagnant; however, the reaction processes continued in the gas mixture. At a temperature of around 600°C, the reaction simultaneously converted all of the dark chemical species into transparent ones everywhere inside the tube.

At a higher pressure (33.8 MPa, 4900 psig), the temperature jumped up to about 600°C immediately after the regression front passed the TC and gradually increased to about 700°C. Then the luminous flame appeared, bringing the temperature up to around 1700°C. Note that the temperature corresponding to start of the transparent zone for tests at different pressures was very close to 600°C.

The same TC temperature measurements were also conducted in feeding tests. As noted previously,[14,22] the XM46 LP exhibits peculiar combustion behavior, such as burnback (also called flashback) characteristics and black cone formation above the liquid/gas interface. The temperature and species profile measurements of the black cone can definitely help the understanding of the burnback phenomena.

In a typical feeding test, the temperature distribution in the reaction zone of the XM46 is shown in Fig. 9. The test was conducted at a pressure of 27.7 MPa and a feeding rate of 10.16 cm/s. For this particular test condition, the cone height was 1.5–1.7 cm. Inside the cone, the temperature was around 300°C. The temperature gradually increased in the top few millimeters, then suddenly jumped to luminous flame temperature. The temperature oscillations started at about 1.4 cm. This oscillation was caused by the fluctuations of the narrow cone tip around the small TC bead. Another interesting observation was that the black cone temperatures at high-pressure tests were roughly the same as the temperatures of dark smoke at low-pressure tests. This implies that the species inside the dark-colored cone could be very similar to those in the dark-smoke zone of the static tests for pressures below 28 MPa.

Pyrolysis Products Analysis

The pyrolysis products of XM46 at different temperatures were analyzed using a Shimadzu QP-5000 GC/MS system. Figure 10 shows the amount of species (in moles) evolved from 0.2 μl of XM46 at different pyrolyzer temperatures from 130 to 540°C. The major product species detected in these tests, listed in the order of decreasing average number of moles evolved, are NO, N_2O, N_2, CO_2, CO, H_2O, HCN, and C_2H_4. As noted in Fig. 10, the amounts

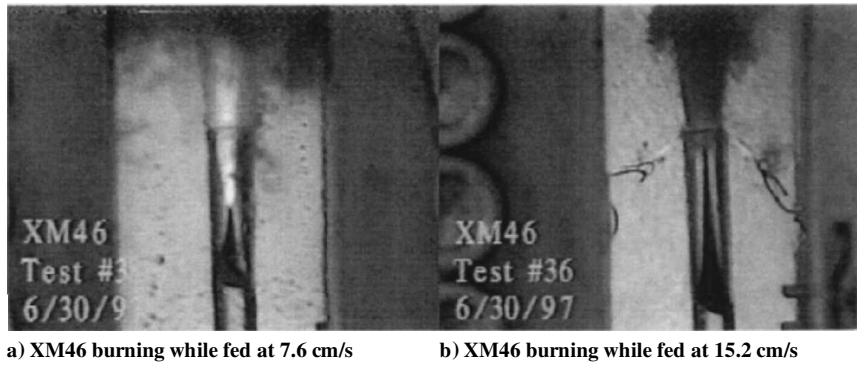

a) XM46 burning while fed at 7.6 cm/s b) XM46 burning while fed at 15.2 cm/s

Fig. 7 Images of XM46 combustion at 27.7 MPa and two different feeding rates.

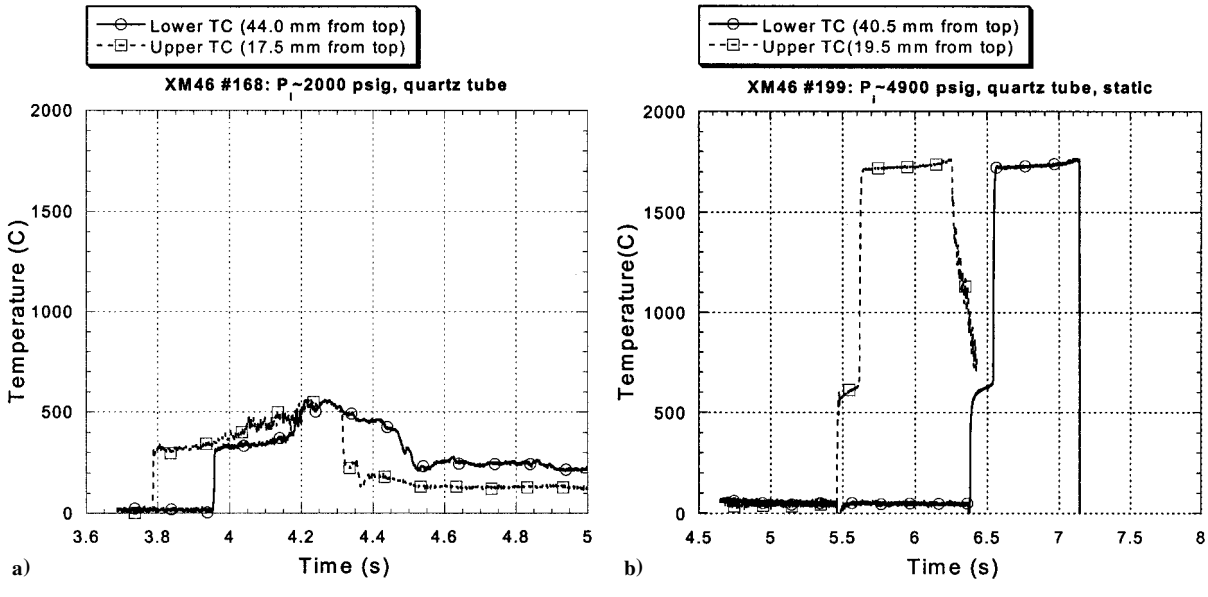

Fig. 8 Temperature distribution inside XM46 reaction zone at low and high pressures.

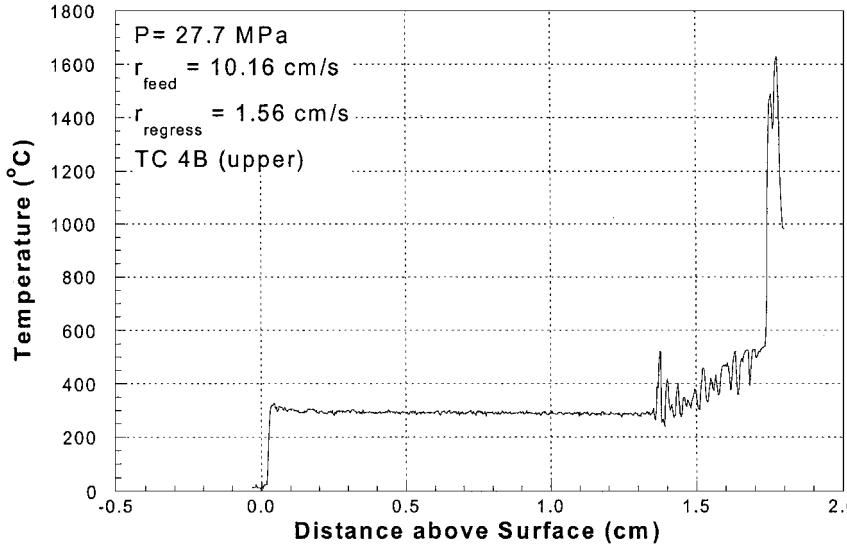

Fig. 9 Temperature distribution of XM46 reaction zone under feeding condition.

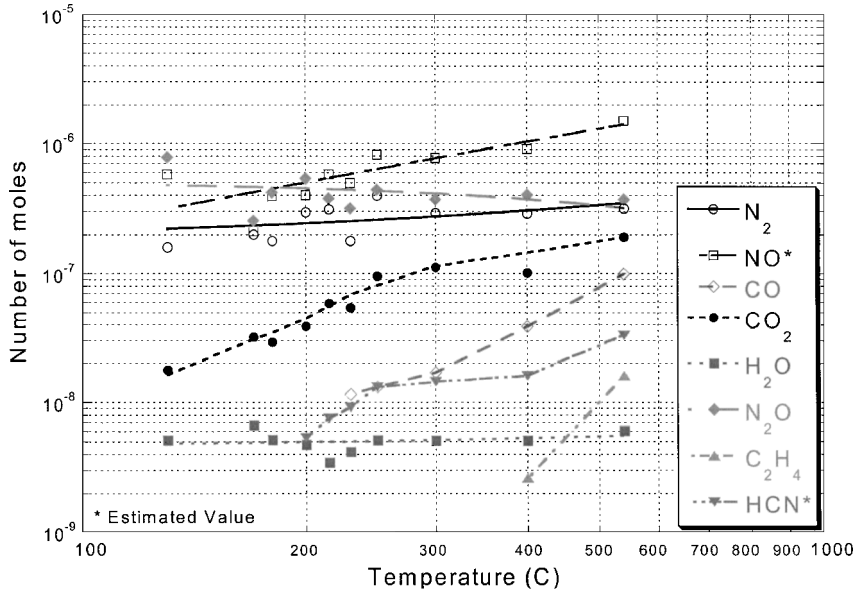

Fig. 10 Mass spectrometer output for pyrolyzed XM46.

of NO and HCN species are approximate values because high concentrations of these toxic gases were not available for calibration. The appearance of NO and N_2O at temperatures as low as 130°C is consistent with what was observed in the pyrolysis tests of HAN–water solutions by Lee and Thynell.[16] NO_2 and HNO_3 were not detectable, due to the limitations of the GC column for NO_2 and of the MS detector for HNO_3. The amounts of four major HAN decomposition species, NO, N_2O, N_2, and H_2O, did not change much with pyrolysis temperature. Carbon-containing species, however, showed a stronger dependence on the pyrolysis temperature. At least an order of magnitude change of the amount over the temperature range from 130 to 540°C was observed for these species. The appearance of carbon-containing species at temperatures below the generally reported TEAN decomposition temperature of 240 to 250°C (Ref. 18) indicated the interaction between TEAN and oxidizing species generated from HAN decomposition.[22] This is also in agreement with the measurements of Lee and Litzinger.[19] As the pyrolysis temperature increased, the oxidation of TEAN by HAN decomposition products became more significant, generating more carbon-containing species. Although two of the major oxidizing species, HNO_3 and NO_2, can not be detected, the decreasing trend of one of the detectable oxidizing species, N_2O, is consistent with the preceding arguments. The decreasing trend of N_2O and increasing trend of NO as the pyrolysis temperature is increased suggest multiple temperature-sensitive reaction pathways. At low temperatures, the decomposition reaction of hyponitrous acid (HO−N=N−OH) to form N_2O and water seems to be more favorable than the reactions involving H−N=O and HO−N=O to form NO and water.

Discussion

Staged Nature of XM46 Combustion

As mentioned in the Introduction and seen in the present study, XM46 LP exhibits staged combustion characteristics. It was proposed in the literature[9–11] that in the reaction zone, HAN decomposed first, followed by a region with mixed HAN decomposition products and dispersed molten TEAN droplets, then the TEAN decomposed and reacted with HAN decomposition products producing a luminous flame. This interpretation, however, has difficulty explaining other phenomena reported in the literature, such as early appearance of carbon-containing species for high heat-flux laser heating experiments.[19] Therefore, one should consider the possibility of the simultaneous TEAN decomposition with HAN. Furthermore, the results from this study on XM46 strongly suggest that TEAN decomposes nearly simultaneously with HAN. As shown in Fig. 10, carbon-containing species were observed in the gas evolved

from the XM46 sample heated to 130°C, which is below the HAN decomposition temperature of 160–170°C. The minimum temperature of 130°C for observing carbon-containing species is also lower than the TEAN decomposition temperature around 240–250°C (Ref. 20).

From the measured temperature plateau around 300°C at pressures up to 17.5 MPa, it can be postulated that the reaction rates in the dark-smoke zone are extremely slow. Because this temperature is higher than the reported TEAN decomposition temperature, it is most likely that there are no intact TEAN molecules in the dark-smoke region.

Another piece of evidence for simultaneous decomposition of TEAN and HAN is the very dark color of the product gases generated from the decomposition reactions. Among many decomposition species of HAN, NO_2 is the only significant source of color, a brown-colored gas. The dark-colored smoke must have substantial contribution from TEAN decomposition products, because TEAN is the only carbon-containing component of XM46. Based on these observations and interpretation, it is a logical deduction that TEAN also participates actively in the initial decomposition stage of XM46.

From this reasoning, it is proposed that the reaction of XM46 consists of the following steps:

1) The initial decomposition of both HAN and TEAN is most likely initiated in the liquid phase, because the temperature gradients in liquid and gas phases are extremely steep and the temperature of the gaseous decomposition products very close to the surface is around 300°C, which is significantly higher than the observed initial decomposition temperature of 130°C. The decomposition products are believed to include brown-colored NO_2 and heavy intermediate opaque carbon-containing species.

2) At low pressures (below 28 MPa), heavy intermediate species can have long residence time before breaking down into transparent molecules. This causes formation of a thick dark-opaque zone above the burning surface. As pressure increases, the residence time decreases, resulting in the reduction of the height of the dark-opaque zone. At around 600°C, all NO_2 and carbon-containing opaque intermediate species have been converted into transparent species.

3) After a short induction period, the reaction between transparent species can produce a steep temperature gradient associated with the appearance of a luminous flame. The duration of the induction period is also a function of pressure.

At very high pressures, the two steep temperature regions can even coalesce into a single temperature jump region.

Mechanism of Burnback Phenomena

The phenomena observed in feeding tests shed insights into the physicochemical processes occurring in the reaction zone. Because the reaction front kept regressing down into the feeding tube no matter how fast the liquid was fed, the net regression speed (surface regression speed plus feeding speed) increased with increasing feeding rate. As shown in Fig. 9, the black-cone temperature was roughly at 300°C, the same as the temperature of the dark smoke (Fig. 8). This suggests that the composition of the species inside the dark cone may be very similar to those of the black smoke seen in lower-pressure static tests. The correspondence of higher burning rate with the existence of either dark smoke in static tests or dark-colored cone in feeding tests indicated the possibility that the burning rate is controlled by the concentration of radicals right above the burning surface. Exactly how the feeding motion increases the concentration of radicals is still unclear at this moment. However, it is safe to postulate that the feeding action enhances the radial motion of the fresh LP and thereby promotes the mixing between unburned and partially reacted liquid.

Controlling Parameters of the Burning Rate

The mechanism through which the pressure affects the burning rate of XM46 is not totally understood. However, some possible controlling mechanisms have been identified after reviewing the results of this investigation together with existing literature.

HAN–water solution, when heated, is known to undergo a series of liquid-phase reactions, as summarized by Lee and Thynell.[16] Therefore, it is reasonable to assume that the decomposition front of XM46 combustion is initiated and controlled by liquid-phase reactions. However, the pressure does not directly affect the species concentrations in the liquid phase. Therefore, pressure affects the burning rate in an indirect manner.

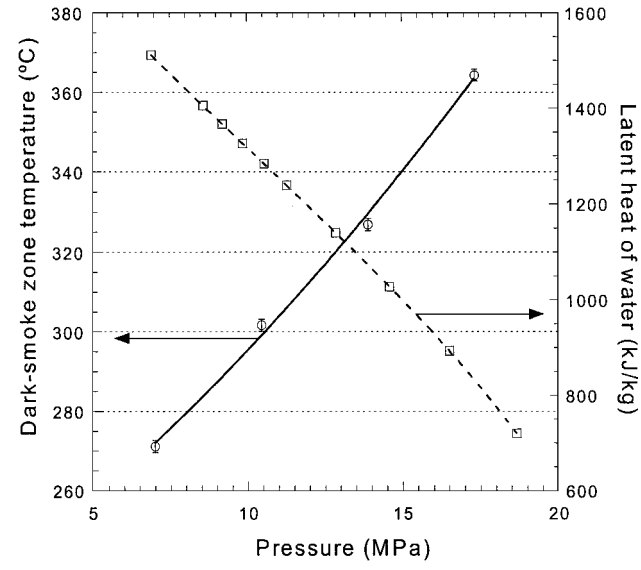

Fig. 11 Variation of dark-smoke temperature and latent heat of water with pressure.

Some possible mechanisms through which the pressure affects the burning rate of XM46 are 1) increasing gas phase heat release rate with increasing pressure; 2) increasing gas-phase heat conduction, and thus heat feedback, with increasing pressure; 3) decreasing latent heat of water with increasing pressure; and 4) increasing gas dissolution rate or decreasing gas desorption rate with increasing pressure. Mechanisms 1 and 2 are generally tied together, because the heat release in the gas phase provides the energy for conductive heat transfer back to the unburned propellant. Unlike the conventional propellant combustion situation, the burning rate of the propellant is a highly nonlinear function of pressure due to its dependency on multiple parameters, including the pressure-dependent latent heat of water, ΔH_v, (see Fig. 11), the enthalpy increase from initial to surface temperature, the conductive heat flux from the gas phase $\dot{q}''_{\text{cond}}$, the net radiative heat flux absorbed at the surface $\dot{q}''_{\text{rad}}$, and the heat release in the surface layer Q_s, as shown by the following simplified energy flux balance equation across the gas/liquid interface:

$$\rho_p r_b \left(\int_{T_i}^{T_s} C_p \mathrm{d}T + \Delta H_v \right) = \rho_p r_b Q_s + \dot{q}''_{\text{cond}} + \dot{q}''_{\text{rad}} \qquad (1)$$

where ρ_p is the propellant density, r_b the burning rate, and C_p the averaged constant-pressure specific heat. At higher pressures, the liquid surface temperature is higher based on the observed trend of the dark-smoke zone temperature shown in Fig. 11. Note that the measured dark-smoke zone temperature is not exactly the surface temperature. However, the surface temperature should follow a similar trend, based on the temperature continuity requirement at the gas/liquid interface.

As shown in Fig. 11, the latent heat of water decreases with increase in pressure. The temperature of the dark-smoke zone increased more than 80°C with increasing pressure in the range from 7 to 17.5 MPa. Because the dark-smoke zone temperature increases with pressure, the enthalpy difference from the initial temperature to the surface temperature should also increase with pressure. The value of Q_s should increase with pressure. As pressure is increased, the temperature within the surface reaction zone increases, thereby promoting the reaction of the decomposition species in the liquid, as well as increasing the collision rate and the heterogeneous reaction rate of gas-phase molecules on the liquid surface. In addition, both the conductive heat flux from the gas phase and the net radiative heat flux absorbed at the surface are functions of pressure.

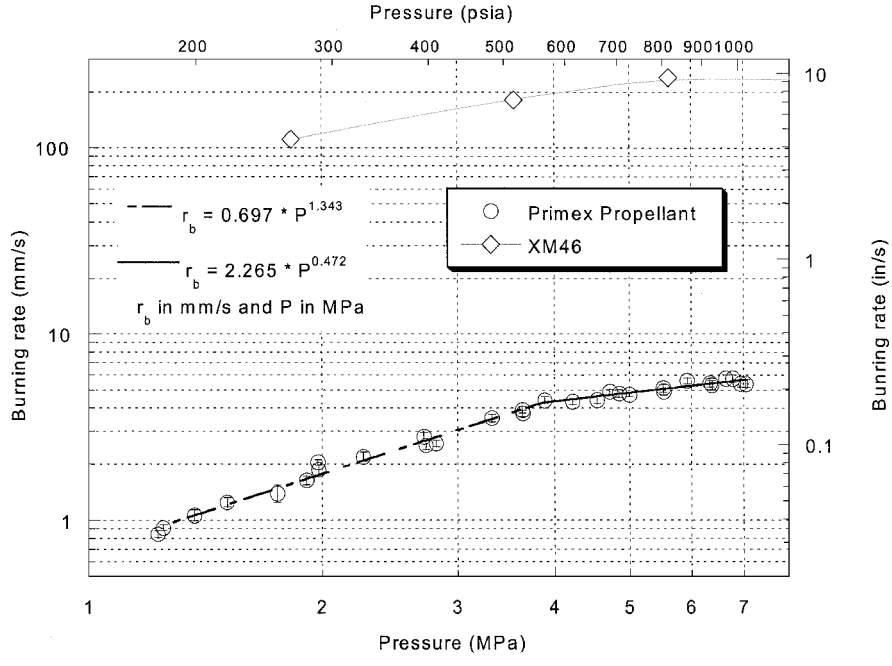

Fig. 12 Burning-rate comparison between XM46 and Primex propellant.

Therefore, Eq. (1) is a highly nonlinear pressure-dependent equation; the burning rate determined from this complex relationship can vary with pressure in a nonconventional manner.

As pointed out by Harting et al.,[25] the evaporation of water can play an important role in HAN-based LPs. The heat released during HAN and TEAN decomposition has to vaporize the water and to increase the sensible enthalpy of the combustion products. Because of the decrease of the latent heat of water with pressure, the sensible enthalpy of the products will be higher. According to the CEA calculation, the total heat of reaction of XM46 combustion is 5116 kJ/kg. However, much of the energy is released in the gas-phase region away from the decomposition front. Therefore, the latent heat of water (1551 kJ/kg at 6.9 MPa) can be a significant portion of the heat release in the decomposition zone.

Also note that the activation energy of solid HAN [47.12 kJ/mol (Ref. 16)], solid TEAN [68.5 kJ/mol (Ref. 20)], and the latent heat of water converted to a molar basis (40.63 kJ/mol at 1 atm) are all on the same order of magnitude. Therefore, the change in the latent heat of water can affect the balance between decomposition and evaporation processes. Other physical processes can also play a role in the burning rate trend of XM46. Surface instability has been identified as one of the controlling mechanisms of the LP apparent burning rates.[10] The decrease of burning rate as pressure was increased from 7 to 28 MPa can be attributed to the suppression of the surface ripples as the gas/liquid density ratio across the interface increased. However, it is hard to explain the burning-rate trends observed at other pressure ranges in this study using the surface instability interpretation alone.

The gas dissolution/desorption process can also affect the burning rate in different ways. First, the dissolution of some gas species could generate radicals to accelerate reactions. For example, the dissolution of NO_2 in water can generate nitrous acid,[26] which is known to enhance the HAN decomposition reactions:

$$2NO_2 + H_2O \rightarrow HNO_2 + HNO_3 \qquad (2)$$

Second, as pressure increases, the product concentration in the gas phase becomes higher; this increases the probability for product gas dissolution gas into the liquid phase, which in turn could retard the forward reaction.

Effect of Fuel Components

Because TEAN also participates in the decomposition reaction, the fuel component can play an important role in the early stage of the combustion event. To illustrate this, another HAN-based propellant, consisting of 60 wt% HAN, 14 wt% glycine [$H_2{-}NCH_2{-}COOH$], and 26 wt% water, was tested to study the effect of fuel component in the combustion of HAN-based LPs. Because the weight fractions of HAN and water in this propellant are comparable with those in XM46, the only significant change is the replacement of TEAN by glycine. This propellant was formulated by engineers at Primex Aerospace Company as one of the candidate monopropellants for space thruster applications. The Primex propellant was tested by this research team using the same static test techniques with a quartz tubes as LP holders over the pressure range of 1.4–7 MPa. The burning rate was found to be lower than that of XM46 by two orders of magnitude, as shown in Fig. 12. Based on limited feeding test results, the burnback phenomenon was also significantly altered with the change of fuel component. It is quite evident that the type of fuel ingredient in the HAN-based LPs can strongly affect the major combustion characteristics.

Conclusions

Based on the experimental observations and measurements, several important conclusions are summarized as follows.

1) The apparent burning rates of XM46 measured with combustible straws increase with pressure when $P < 7$ MPa, decrease with pressure when $7 < P < 28$ MPa, remain nearly constant when $28 < P < 100$ MPa, and increase again when $P > 100$ MPa. The luminous flame was observed only when the pressure is above 28 MPa.

2) XM46 exhibits staged-combustion behavior as follows.

a) Decomposition of HAN and TEAN initiate in the liquid phase, producing dark-colored gaseous products (including NO_2 and large carbon containing species) at temperatures around 300°C near the LP surface.

b) Breakdown of heavy intermediate opaque species into transparent molecules occurs around 600°C.

c) Final reactions between transparent species produce a luminous flame. Similar combustion stages were observed over the pressure range tested, though the heights of different zones varied with pressure.

3) The burnback phenomenon is believed to be the result of interaction between the pyrolyzed radical species and LP near the surface. Surface agitation and radial motion of the liquid due to feeding can definitely enhance the reactions resulting in the flashback behavior.

4) Pyrolysis tests of XM46 were conducted in a specially designed pyrolyzer used in conjunction with a GC/MS. The major pyrolysis

products observed were NO, N_2O, N_2, CO_2, CO, H_2O, HCN, and C_2H_4 when pyrolyzed at temperatures between 130 and 540°C.

5) A number of physicochemical processes that could have significant influence on burning characteristics of the HAN-based LP were considered. Unlike the conventional solid-propellant combustion situation, the pressure dependency of the burning rate of the HAN-based LP cannot be represented by a simple function. Water evaporation below the critical point seems to have a noticeable effect on combustion characteristics of XM46 because the latent heat is on the same order of magnitude with HAN and TEAN activation energy and the amount of heat release in the decomposition zone. Gas dissolution/desorption could also affect the burning rate.

6) The type of fuel ingredient in HAN-based liquid monopropellant could have a significant effect on the overall burning characteristics, as demonstrated by the replacement of TEAN with glycine.

Acknowledgments

This work has been sponsored by the Army Research Office (Contract DAAH04-96-1-0054) under the management of David M. Mann, with partial support from Gloria Wren of the Army Research Lab (ARL). The generosity of Avi Birk of ARL in providing us with the High Pressure Windowed Chamber is greatly appreciated. The effort on the burning rate measurement of the Primex propellant was funded by Primex Aerospace Company through a NASA John H. Glenn Research Center at Lewis Field project. The authors would like to thank Dennis Meinhardt and E. J. Wucherer of Primex as well as Brian Reed of NASA Glenn Research Center for their support. The efforts of BaoQi Zhang for the experimental work on the Primex liquid propellant and Donald Koch's help on this project are greatly appreciated.

References

[1]Klein, N., "Liquid Propellants for Use in Guns," *Gun Propulsion Technology*, edited by L. Stiefel, Vol. 109, Progress in Astronautics and Aeronautics, AIAA, Washington, DC, 1988, Chap. 14.

[2]Morrison, W. F., and Knapton, J. D., "Liquid Propellant Guns," *Gun Propulsion Technology*, edited by L. Stiefel, Vol. 109, Progress in Astronautics and Aeronautics, AIAA, Washington, DC, 1988, Chap. 13.

[3]Palaszewski, B., Ianoski, I. A., and Carrick, P., "Propellant Technologies: Far-Reaching Benefits for Aeronautical and Space-Vehicle Propulsion," *Journal of Propulsion and Power*, Vol. 14, No. 5, 1998, pp. 641–648.

[4]Sackheim, R. L., and Byers, D. C., "Status and Issues Related to In-Space Propulsion Systems," *Journal of Propulsion and Power*, Vol. 14, No. 5, 1998, pp. 669–675.

[5]Hurlbert, E., Applewhite, J., Nguyen, T., Reed, B., Zhang, B., and Wang, Y., "Nontoxic Orbital Maneuvering and Reaction Control Systems for Reusable Spacecraft," *Journal of Propulsion and Power*, Vol. 14, No. 5, 1998, pp. 676–687.

[6]Meinhardt, D., Brewster, G., Christofferson, S., and Wucherer, E. J., "Development and Testing of New, HAN-Based Monopropellants in Small Rocket Thrusters," AIAA Paper 98-4006, July 1998.

[7]Oberle, W. F., and Wren, G. P., "Burn Rates of LGP 1846 Conditioned Ambient, Hot, and Cold," U.S. Army Research Lab., Rept. BRL-TR-3287, Aberdeen Proving Ground, MD, Oct. 1991.

[8]McBratney, W. F., and Vanderhoff, J. A., "High Pressure Windowed Chamber Burn Rate Determination of Liquid Propellant XM46," U.S. Army Research Lab., Rept. ARL-TR-442, Aberdeen Proving Ground, MD, 1994.

[9]Vosen, S. R., "The Burning Rate of Hydroxylammonium Nitrate-Based Liquid Propellants," *Proceedings of the Twenty-Second Symposium (International) on Combustion*, Combustion Inst., Pittsburgh, PA, 1988, pp. 1817–1825.

[10]Vosen, S. R., "Concentration and Pressure Effects on the Decomposition Rate of Aqueous Hydroxylammonium Nitrate Solutions," *Combustion Science and Technology*, Vol. 68, Nos. 4–6, 1989, pp. 85–99.

[11]Vosen, S. R., "Hydroxylammonium Nitrate-Based Liquid Propellant Combustion—Interpretation of Strand Burner Data and the Laminar Burning Velocity," *Combustion and Flame*, Vol. 82, Nos. 3–4, 1990, pp. 376–388.

[12]Koch, D., Lu, Y. C., Kuo, K. K., and Jones, E., "Design & Development of a Liquid Propellant Strand Burner with Initial Application to Nitromethane," *Proceedings of the 33rd JANNAF Combustion Subcommittee Meeting*, CPIA Publ. 653, Vol. 1, Chemical Propulsion Information Agency, Laurel, MD, 1996, pp. 127–135.

[13]Boyer, E., and Kuo, K. K., "Flame Structure and Combustion Behavior of Nitromethane," *Proceedings of the 35th JANNAF Combustion Subcommittee Meeting*, CPIA Pub1. 680, Vol. 1, Chemical Propulsion Information Agency, Laurel, MD, 1998, pp. 699–706.

[14]Jennings, S. T., Chang, Y. P., Koch, D., and Kuo, K. K., "Peculiar Combustion Characteristics of XM46 Liquid Propellant," *Proceedings of the 34th JANNAF Combustion Subcommittee Meeting*, CPIA Publ. 662, Vol. 1, Chemical Propulsion Information Agency, Laurel, MD, 1997, pp. 321–333.

[15]Klein, N., "Ignition and Combustion of the HAN-Based Liquid Propellants," *Proceedings of the 27th JANNAF Combustion Subcommittee Meeting*, CPIA Publ. 557, Vol. 1, Chemical Propulsion Information Agency, Laurel, MD, 1990, pp. 443–450.

[16]Lee, H. S., and Thynell, S. T., "Confined Rapid Thermolysis/FTIR Spectroscopy of Hydroxylammonium Nitrate," AIAA Paper 97-3232, July 1997.

[17]Thynell, S. T., and Kim, E. S., "The Effect of Pressure on the Thermal Decomposition Characteristics of Hydroxylammonium Nitrate," *Proceedings of the 35th JANNAF Combustion Subcommittee Meeting and 17th Propulsion System Hazards Subcommittee Meeting, Joint Sessions*, CPIA Publ. 685, Chemical Propulsion Information Agency, Laurel, MD, 1998, pp. 47–59.

[18]Cronin, J. T., and Brill, T. B., "Thermal Decomposition of Energetic Materials 29—The Fast Thermal Decomposition Characteristics of a Multicomponent Material: Liquid Gun Propellant 1845," *Combustion and Flame*, Vol. 74, No. 1, 1988, pp. 81–89.

[19]Lee, Y. J., and Litzinger, T. A., "Combustion Chemistry of HAN, TEAN, and XM46," *Combustion Science and Technology*, Vol. 141, Nos. 1–6, 1999, pp. 19–36.

[20]Beyer, R. A., "Shock Tube Study of the Reaction of Triethanol Ammonium Nitrate with N_2O," *Proceedings of the 27th JANNAF Combustion Meeting*, CPIA Publ. 557, Vol. 1, Chemical Propulsion Information Agency, Laurel, MD, 1990, pp. 605–609.

[21]Schoppelrei, J. W., Kieke, M. L., and Brill, T. B., "Spectroscopy of Hydrothermal Reactions. 2. Reactions and Kinetic Parameters of $[NH_3OH]NO_3$ and Equilibria of $(NH_4)_2CO_3$ Determined with a Flow Cell and FT Raman Spectroscopy," *Journal of Physical Chemistry*, Vol. 100, No. 18, 1996, pp. 7463–7470.

[22]Chang, Y. P., Boyer, E., Yeh, C. L., Kuo, K. K., and Jennings, S. T., "Combustion Behavior of XM46 Liquid Propellant," *Proceedings of the 24th International Pyrotechnics Seminar*, IIT Research Inst., Chicago, 1998, pp. 625–635.

[23]Boyer, E., and Kuo, K. K., "High Pressure Combustion Behavior of Nitromethane," AIAA Paper 99-2358, June 1999.

[24]Lee, T.-W., Tseng, L.-K., and Faeth, G. M., "Separated-Flow Considerations for Pressure-Atomized Combusting Monopropellant Sprays," *Journal of Propulsion and Power*, Vol. 6, No. 4, 1990, pp. 382–391.

[25]Harting, G. C., Mordosky, J. W., Zhang, B. Q., Cook, T. T., and Kuo, K. K., "Burning Rate Characterization of OXSOL Liquid Oxidizer," *Combustion of Energetic Materials*, edited by K. K. Kuo and L. T. De Luca, Begell House, New York, (to be published).

[26]Leveritt, C. S., Bunte, S. W., and Klein, N., "Hydroxylammonium Nitrate (HAN) Liquid Propellant Stability Enhancement," Army Research Lab., Rept. ARL-TR-2037, Aberdeen Proving Ground, MD, Sept. 1999.